Microgravity Science and Technology (2022) 34: 59
https://doi.org/10.1007/s12217-022-09980-1

ORIGINAL ARTICLE

Multi-channel Thermal Deformation Interference Measurement of the Telescope Supporting Frame in Spaceborne Gravitational Wave Detection

Jia Shen[1,3] · Ya Zhao[4] · Heshan Liu[1,2] · Yu Niu[1,2] · Ruihong Gao[5] · Tong Guo[6] · Donglin Zhao[7] · Ziren Luo[1,2]

Received: 10 March 2022 / Accepted: 24 June 2022 / Published online: 13 July 2022

Abstract

The Taiji program and the LISA (Laser Interferometer Space Antenna) program are proposed to realize the gravitational wave detection within the frequency band of 0.1 mHz-1 Hz through space laser interferometry. As a key optical component of the interferometric system, the telescope are required the dimensional stability better than 1 pm/$\sqrt{\text{Hz}}$ and its deformation between the primary and the secondary mirrors needs to be small enough to reduce wavefront distortion. Therefore, in the case of satisfying the structural strength, the telescope supporting structural material also needs to meet the performance of the low coefficient of thermal expansion (CTE) and high thermal conductivity. In this paper, we fabricate a telescope supporting frame using the carbon/silicon carbide (C/SiC) composite, and build a high-precision and multi-channel thermal deformation interferometry system. Using this system, the uniform thermal expansion experiment and the temperature gradient thermal expansion experiment are carried out on the telescope supporting frame. The results show that the axial CTE and the transverse CTE of the C/SiC composite is about -8.3×10^{-7}/K and 3.3×10^{-5}/K, respectively, which indicate that the design and process of the C/SiC composite used may not be mature and need to be further studied. The high-precision multi-channel thermal deformation measurement interferometry system designed in this paper can be used for the subsequent thermal performance measurement of the telescope prototype.

Keywords Coefficient of thermal expansion (CTE) · Interferometry · Multi-channel · Carbon/silicon carbide(C/SiC) · Telescope

TC: Pioneer WR Hu - Research Pioneer and Leader of Microgravity Science in China: Dedicated to the 85th Birthday of Academician Wen-Rui Hu
Guest Editors: Jian-Fu Zhao, Kai Li

✉ Yu Niu
niuyu@imech.ac.cn

Jia Shen
shenjia@imech.ac.cn

Ya Zhao
zhaoya16@mails.ucas.edu.cn

Heshan Liu
liuheshan@imech.ac.cn

Ruihong Gao
gaoruihong@imech.ac.cn

Tong Guo
guot1608@126.com

Donglin Zhao
zhaodonglin0@nwpu.edu.cn

Ziren Luo
luoziren@imech.ac.cn

[1] Center for Gravitational Wave Experiment, National Microgravity Laboratory, Institute of Mechanics, Chinese Academy of Sciences, 100190 Beijing, China

[2] Taiji Laboratory for Gravitational Wave Universe (Beijing/Hangzhou), University of Chinese Academy of Sciences, Beijing 100049, China

[3] School of Engineering Science, University of Chinese Academy of Sciences, Beijing 100049, China

[4] Changchun Institute of Optics, Fine Mechanics and Physics, Chinese Academy of Sciences, Changchun 130033, China

[5] School of Fundamental Physics and Mathematical Sciences, Hangzhou Institute for Advanced Study, UCAS, Hangzhou 310024, China

[6] Innovation Academy for Microsatellites of Chinese Academy of Sciences, Shanghai 201304, China

[7] Northwestern Polytechnical University, Xian 710072, China

Introduction

The space-borne and long-baseline laser interferometers such as the Laser Interferometer Space Antenna (LISA) Bender and Danzmann (1998) and Taiji program Luo et al. (2020); Hu and Wu (2017); Luo et al. (2021), aim to detect the gravitational waves in the frequency band within 0.1 mHz ∼ 1 Hz. There are three SC (spacecraft) forming an equilateral triangle with arm lengths of millions of kilometers, and each SC has two telescopes, which collimates and expands the 1064 nm laser beam from the local optical bench and sends it to a distant spacecraft Livas and Sankar (2016); Livas et al. (2013); Sasso et al. (2018); Sankar and Livas (2014); Livas and Sankar (2015). In order to successfully detect the gravitational waves, optical path stability of the detectors needs to meet 1 pm/$\sqrt{\text{Hz}}$. As the key device of transmitting beam, the structural stability of the telescope is pretty critical. And the thermal environment of the telescope has large applied gradients that may lead to the decline of the optical performance of the telescope. The aforementioned factors result in the use of highly stable material for building the structure of the telescope.

Silicon carbide (SiC) has the characteristic of high thermal conductivity which can minimize the temperature gradients of the in-orbit telescope structure, but its coefficient of thermal expansion (CTE) of 10^{-6} magnitude makes a risk to meet the optical path stability of 1 pm/$\sqrt{\text{Hz}}$ Sanjuan et al. (2012); Sankar and Livas (2016). The advantage of carbon fiber reinforced polymer (CFRP) is that the CTE can be adjusted to be near zero, but its in-orbit performance is limited due to the water shrinkage and the low thermal conductivity Sanjuan et al. (2011); Machado et al. (2008). At present, SiC and CFRP are chosen as the candidates and studied by researchers. Carbon/silicon carbide (C/SiC) composite not only has the advantage that CTE can be tuned, but also has better anti-shrinkage property and higher thermal conductivity than CFRP. Therefore, it is also worth joining the ranks of research. A frame structure with the height of about 315 mm is made of C/SiC composite in our paper, and a high-precision three-channel symmetrical interferometry system has been built to measure the CTE of the structure at room temperature. Both the uniform thermal expansion and the thermal expansion with the temperature gradient are processed to characterize the thermal properties of C/SiC composite.

The paper is organized as follows. "Experimental Setup" focuses on the experimental setup together with the experimental scheme design, optical mechanical design and thermal design. Experimental measurements of the uniform thermal expansion and the thermal expansion with the temperature gradient are introduced and the results are analyzed in "Experimental Results and Analysis". Main conclusions and the future prospects are summarized in "Conclusion".

Experimental Setup

The tested structure is shown in Fig. 1, which consists of different plates with sedimentation technology. In order to increase the strength of the structure, each corner of the upper and lower parts of the structure is fixed with titanium alloy. For the improvement of the accuracy of the measurement, the displacements in three different positions of the structure are simultaneously measured.

A highly sensitive and symmetric heterodyne interferometer is built to measure the resulting dimensional change of the structure. Its schematic is shown in Fig. 2. The laser source of this interferometer is a non-planarring-oscillator (NPRO) Nd:YAG laser at the wavelength of 1064 nm. And the heterodyne frequency used is $f_1 - f_2 = 1.6$ MHz, which is generated by two Acoustic Optical Modulators (AOMs) working at 130 MHz and 130 MHz + 1.6 MHz, respectively. Two interference beams with frequency f_1 and f_2 are then coupled into the fiber collimators and sent to the test bench with the waist diameters of 1.5 mm. The resulting interference signal is processed by a digital phasemeter, based on a field programmable gate array (FPGA), enabling the measurement accuracies of the setup in the order of pm/$\sqrt{\text{Hz}}$ in displacement. Here we use one of the measurement optical paths as an example to illustrate the readout process of the structural thermal deformation. Assuming that the beat frequency signal generated by the measurement beam reflected from M11 and the reference beam is:

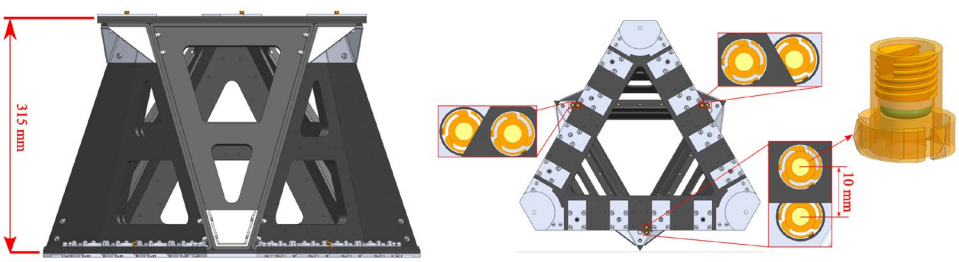

Fig. 1 The CAD model of the C/SiC supporting frame

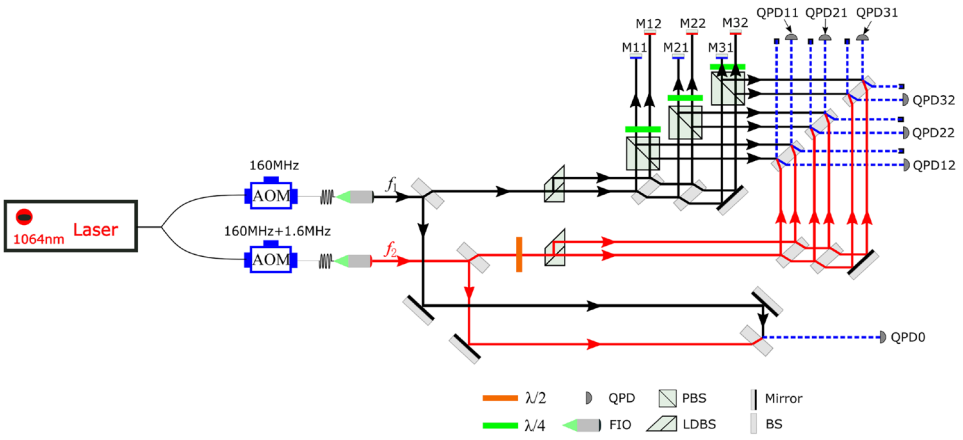

Fig. 2 Schematic of the heterodyne interferometer. AOM = Acoustic Optical Modulator, FIO = Fiber collimator, QPD = Quadrant Photodiode, BS = Beamsplitter, PBS = Polarization beamsplitter, LDBS = Lateral displacement beamsplitter

$$I_{11} = E_{11}\cos(\omega t + \phi_{11}(t)) \tag{1}$$

The beat signal generated by the measurement beam reflected from M12 and the reference beam is:

$$I_{12} = E_{12}\cos(\omega t + \phi_{12}(t)) \tag{2}$$

where I_{11}, I_{12}, E_{11}, E_{12}, $\phi_{11}(t)$, $\phi_{12}(t)$ and $\omega = 2\pi \times (f_1 - f_2)$ denote the strength of the beat signal, the amplitude of the beat signal and the phase change functions of the M12 and M22 mirrors over time caused by the thermal expansion, and the frequency of the beat signal, respectively, which can be obtained through a phasemeter. Therefore, the phase difference between the two mirrors can be expressed as:

$$\Delta\phi_1(t) = \phi_{11}(t) - \phi_{12}(t) \tag{3}$$

Therefore, the displacement change between the two mirrors due to the thermal expansion can be expressed as:

$$\Delta S_1(t) = \frac{\Delta\phi_1(t)}{2k} = \frac{4\pi}{\lambda}\Delta\phi_1(t) \tag{4}$$

Optomechanical Design

The relationship between the laser frequency jitter optical path noise δl and optical path difference (OPD) δs is:

$$\delta l = \frac{\delta v}{v}\delta s \tag{5}$$

where δv is the laser frequency jitter noise, $v = \frac{c}{\lambda}$ is the laser frequency, v and δv of the laser used is about 281 THz and 10 MHz, respectively. If δl is less than 1 pm, δs needs to be less than 3 mm. As shown in Table 1, a common compensation optical path is added during the transmission of the two reference beams, so that the absolute value of the OPD between the two parallel reference beams and the two parallel measurement beams reflected by the upper and lower mirrors is consistent in the optical path design.

As shown in Fig. 1, when measuring the thermal deformation of the supporting frame, it is necessary to calibrate the position of the upper or lower end of the structure through two mirrors. Thus, the Invar clamping device is elaborately designed for installing the mirror, as depicted in Fig. 3. The clamping device is fixed through the interference fit of its three bump with the hole. And the mirror surface is coincided with the surface of the three bumps to ensure that the thermal deformation of the clamping device does not change the position of the mirror, which provides a significant guarantee for the interferometry system to realize the high-precision measurement. In addition, through fine-tuning the attitude of the clamping device, the angle of the reflected beam can be adjusted to facilitate the installation and adjustment of the interference optical path.

Table 1 The optical path and OPD of two interference beams in each interference optical path of the interferometric optical system

	Measurement path 1		Measurement path 2		Measurement path 3	
Detector	QPD11	QPD12	QPD21	QPD22	QPD31	QPD32
Reference path [mm]	2291	2305	2656	2671	2169	2184
Measurement path [mm]	1976	2620	2971	2356	1855	2499
OPD [mm]	315	-315	-315	315	315	-315

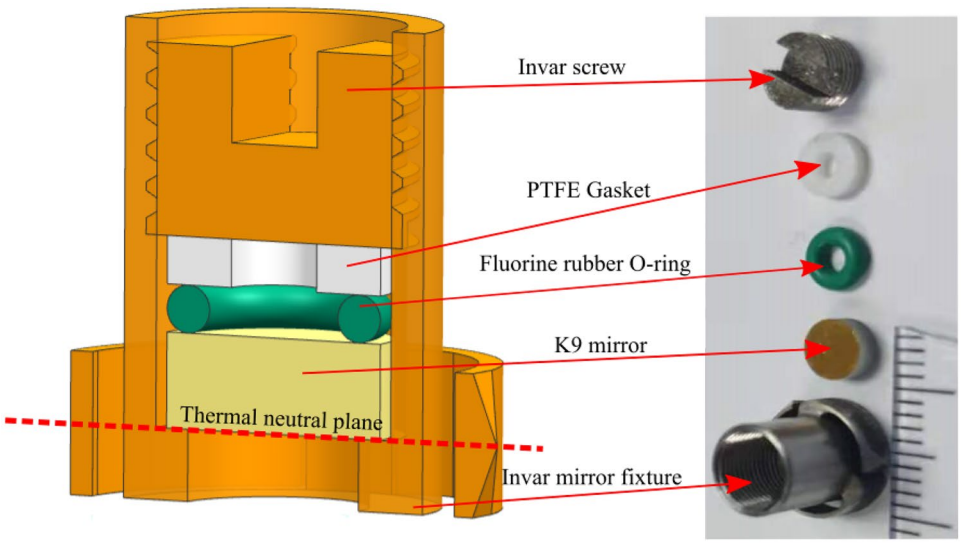

Fig. 3 The CAD model of the clamping device

Thermal Design

As shown on the left of Fig. 4, the heating of the structure is realized by pasting the heating plate on the structure to be tested. In order to ensure the uniformity of the temperature, the heating plate is triangularly symmetrically pasted on the structure to be tested, and the adiabatic coating is utilized to wrap the whole structure (as shown on the right of Fig. 4). At the same time, the temperature measurement points T1 ~ T16 is placed in each position of the structure to monitor the temperature of the corresponding part of the structure in real time. Among them, T1 ~ T3 and T4 ~ T16 are distributed near the three measuring holes at the upper and lower end of the structure, respectively, and T7 ~ T16 are distributed on the supporting surface in the middle of the structure.

In the early temperature debugging, the timer mode of the DC power supply was used to realize the intermittent heating of the structure. We tried to ensure the uniform rise and fall of the temperature of the structure to be tested through adjusting the heating power and heating time of the heating plates at the different positions constantly, obtaining the temperature curve with periodic changes.

Experimental Results and Analysis

After integrating the interferometer measurement system with the structure to be tested, the six mirrors on the structure are fine-tuned so that the two interference beams in each interferometer coincide for obtaining the interference signal with a high signal-to-noise ratio. The final test system

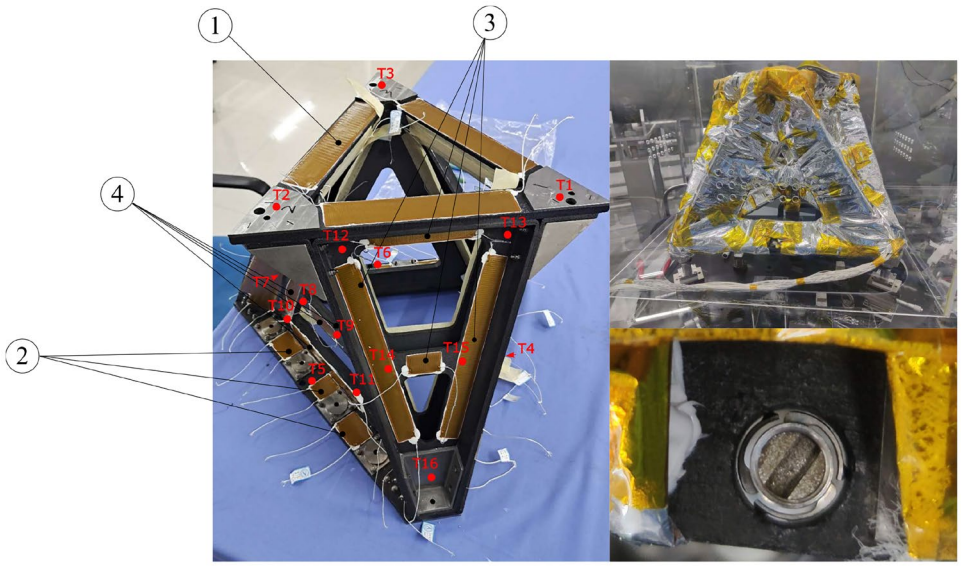

Fig. 4 The thermal design of the C/SiC supporting frame

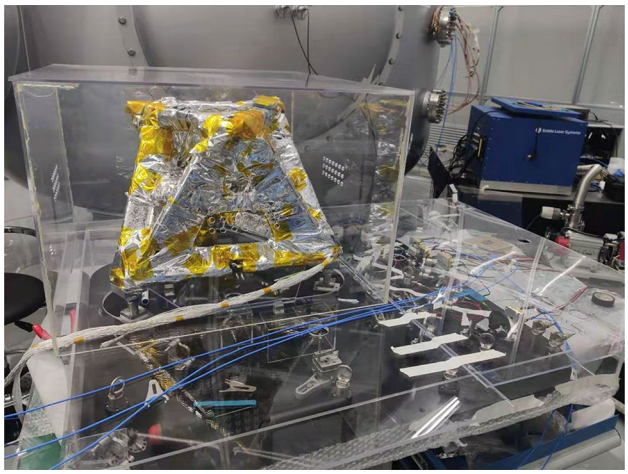

Fig. 5 The experimental scene of the thermal deformation measurement interferometry system

is shown in Fig. 5. Before the formal measurement, we need to conduct an overall system test to obtain the noise level of the measurement system. After the continuous measurement for 10 hours without temperature control, the power spectral density curves of the optical path noise in three-way interferometry $\Delta S1$, $\Delta S2$ and $\Delta S3$ are shown in Fig. 6. We can find that the optical path noise is less than 100 pm when $f \geq 1$ Hz and the optical path noise is less than 100 nm when $f \geq 10^{-2}$ Hz. Since the measurement system has neither been placed on the vibration isolation platform nor in the vacuum chamber, the noise sources mainly come from the mechanical vibration and the air flow. Despite the condition, the results show that the accuracy of the measurement system satisfies the current measurement requirements.

Experimental Measurement of the Uniform Thermal Expansion

Because of the large supporting structure, it is unrealistic to achieve perfect uniform thermal expansion, and the

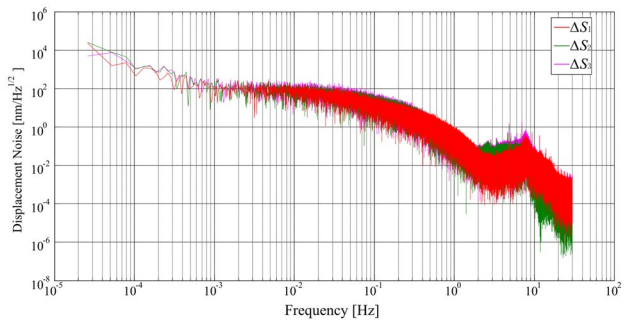

Fig. 6 The power spectral density curve of the optical path noise in three-way interferometry

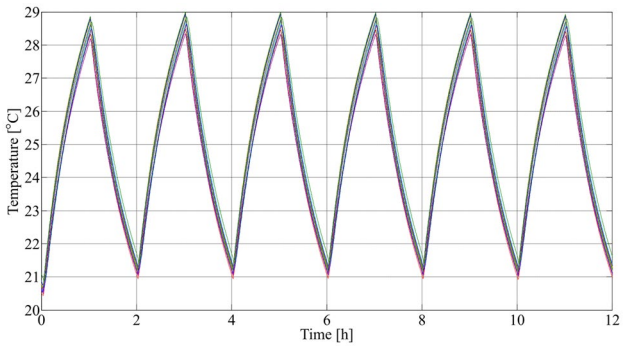

Fig. 7 The periodic temperature rise and fall of the measured structure

temperature consistency between the various temperature measurement points on the structure can only be achieved well through the continuous debugging.

Using the timer function of the DC power supply, the structure can be intermittently heated and released. In the final test process, after the continuous iterative debugging, the period of the temperature change was set to 2 hours, and the rise and fall time of the temperature were both set to 1 hour. The low temperature is set at around 21 °C, and the high temperature is set at around 29 °C. The final temperature fluctuations measured through the 16 temperature measurement points are shown in Fig. 7, and the relative temperature difference of the 16 measurement points at each moment can be guaranteed to be within 0.8 °C, so as to ensure the uniformity of the thermal deformation of the structure to be tested.

We take the average of the temperatures of the whole measurement points to characterize the temperature change of the entire structure, and the result is shown in Fig. 8. Since the exothermic process of the structure dissipates heat to the outside by means of the heat transfer at the room temperature, the temperature fluctuation curve and the corresponding displacement change curve are not perfect sine functions. And the higher the temperature in the rising process, the

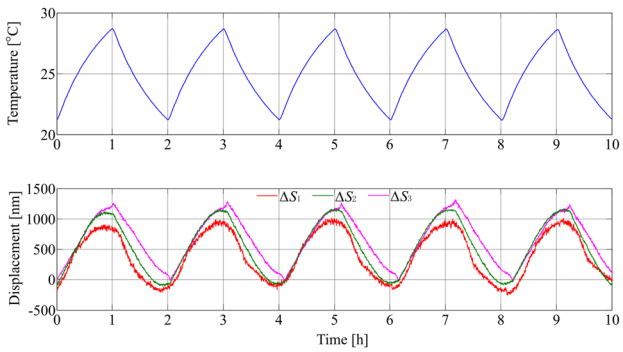

Fig. 8 The experimental results of the uniform thermal expansion

higher the heat transfer efficiency to the surroundings. Thus, the temperature rise curve slows down with the increase of temperature. Similarly, the lower the temperature during the fall, the lower the heat transfer efficiency to the surroundings, so the temperature drop curve slows down with the decrease of temperature.

We take the temperature change curve as the x-axis and the displacement change curve as the y-axis to obtain the hysteresis curve of the displacement change with respect to the temperature change as illustrated in Fig. 9, which is fitted by the linear regression. Then through the formula:

$$\mathrm{CTE_S} = \frac{\mathrm{k}}{2\mathrm{H}} \tag{6}$$

here, k is the slope of the fitting straight line, and H is the distance between the upper and lower mirrors. The measured CTE of the three measurement paths is $2.19 \times 10^{-7}/\mathrm{K}$, $2.32 \times 10^{-7}/\mathrm{K}$, $2.55 \times 10^{-7}/\mathrm{K}$, respectively.

Experimental Measurement of the Thermal Expansion with the Temperature Gradient

In this experiment, we realized the temperature gradient of the structure from top to bottom by only supplying power to the thermal resistance on the top surface of the supporting frame. Compared with the uniform thermal expansion in the previous section, the debugging process of temperature gradient thermal expansion is easier. In order to provide more experimental data for analysis, we carried out three thermal expansion experiments with different temperature gradient.

The results of the first experiment are shown in Fig. 10a, where the temperature is raised for 1 hour and cooled for 1 hour. It is obvious that the temperature gradient of the structure is from the top to the bottom, and the highest and the lowest temperature curve represent the temperature change on the upper and the lower end of the structure, respectively. The maximum temperature gradient is about 4 °C. Since the process of the heat transfer takes some time, it can be seen that there is a delay in the temperature change process

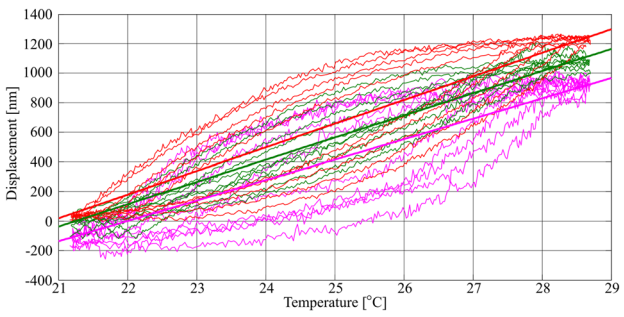

Fig. 9 The hysteresis curve of the displacement change with respect to the temperature change

from the top to the bottom. The lower part of Fig. 10a shows the measured optical length change results of the three-way interference optical path. The consistency between the displacement change curve and the temperature change curve can be clearly seen through the upper and lower comparison. Similarly, the results of the second experiment, as illustrated in Fig. 10b, show that the maximum temperature gradient achieved is about 5 °C. The results of the third experiment are shown in Fig. 10c, the time used for the temperature rise and fall cycle of this experiment is different from that of the previous two experiments, about 1.7 hours, and the realized temperature gradient is around 18 °C.

The variation curve of the temperature gradient of the structure is obtained by subtracting the temperature curve of the lower end surface from that of the upper end surface of the structure, which is served as the x-axis to obtain the hysteresis curve of the displacement change with respect to the temperature change. The fitting results of the three experimental data are shown in Fig. 11a, b, c, respectively.

The accurate maximum temperature gradients of the three experiments are 3.7 °C, 5.2 °C, and 18.5 °C, respectively. At the same time, we notice that the temperature of the lower end surface of the structure also fluctuates periodically within a certain range. This means that the thermal expansion of the structure can be divided into two parts. One is the thermal deformation caused by the upper and lower temperature gradients analyzed above, and the other part is the thermal deformation caused by the uniform expansion, which can be regarded as the result of the temperature fluctuations at the lower end of the structure. Therefore, the measured thermal deformation ΔS an be expressed as:

$$\Delta S = 2 \times \mathrm{CTE} \times \mathrm{H} \times \left(\frac{\mathrm{TG}}{2} + \delta T\right) = k \times (\mathrm{TG} + 2 \times \delta T) \tag{7}$$

where, TG represents the temperature gradient, and δT is the temperature fluctuation at the lower end of the structure. In the analysis of Fig. 11, only the temperature gradient TG is taken as the x-axis, but δT is not taken into account. Therefore, the coefficient after the linear fitting needs to be multiplied by the scale factor $\mathrm{TG}/(\mathrm{TG} + \delta\mathrm{T})$. As shown in Fig. 12, in the three experiments, δT are 0.40 °C, 0.52 °C, and 1.40 °C, respectively. So the calculated scale factors are 0.82, 0.83 and 0.86, respectively. In summary, the slope k obtained by each interferometric measurement in each experiment and the corresponding CTE are shown in Table 2.

Discussion and Analysis

In the uniform thermal expansion experimental measurement, the error between the three-way measurement results is 5%. In the experimental measurement of the thermal expansion deformation with the temperature gradient, the

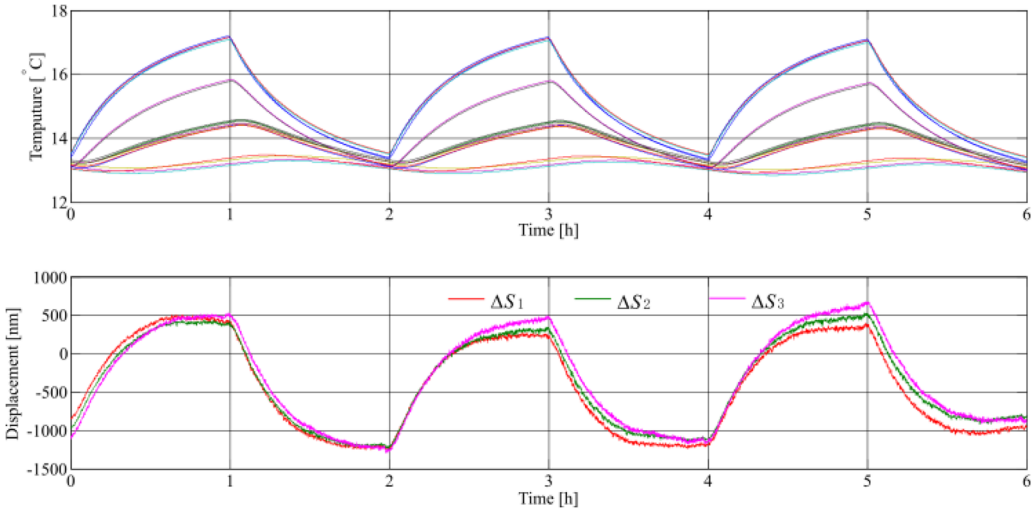

(a) First experimental result

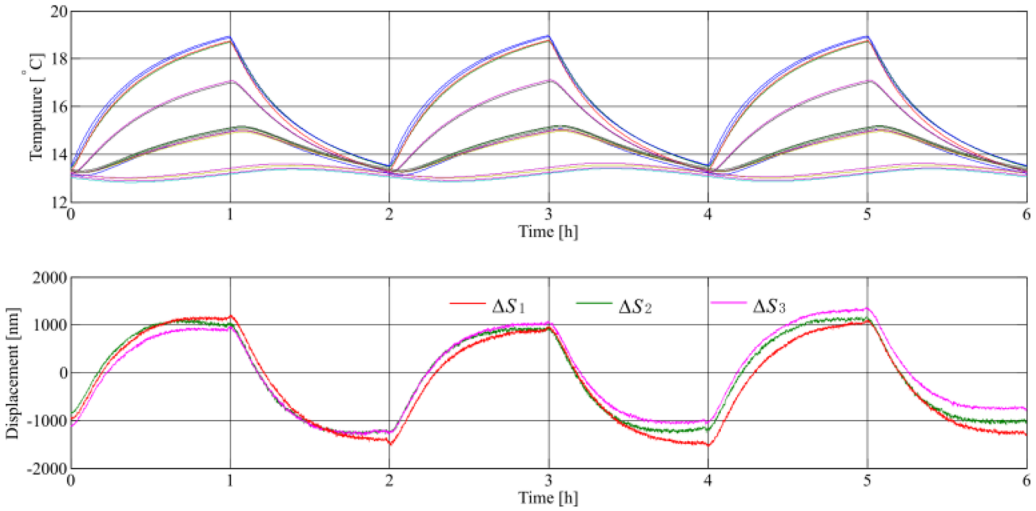

(b) Second experimental result

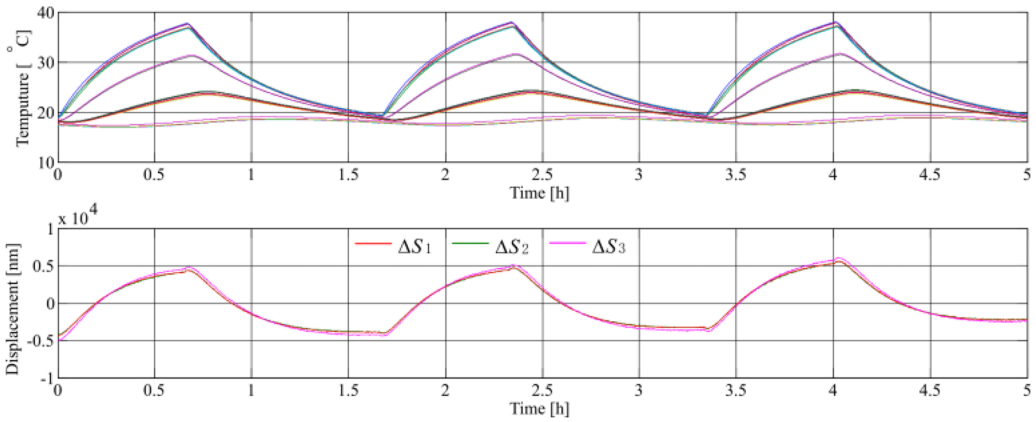

(c) Third experimental result

Fig. 10 The experimental results of the thermal expansion with the temperature gradient

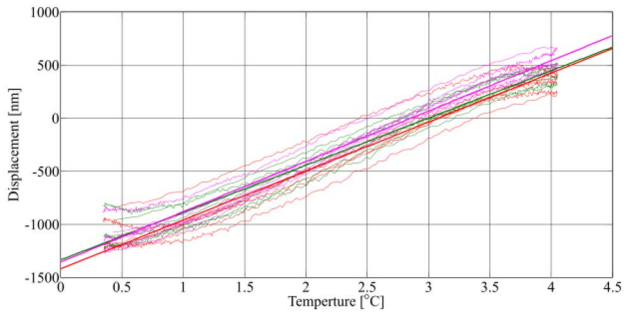

(a) First experimental result.

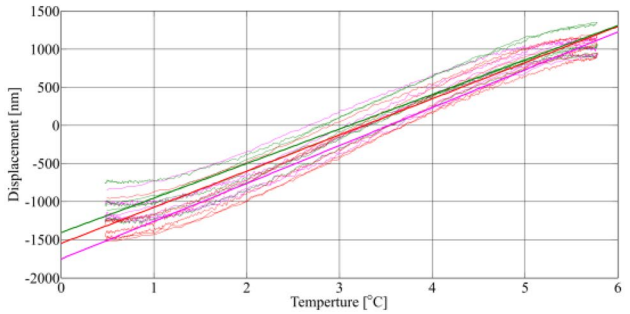

(b) Second experimental result.

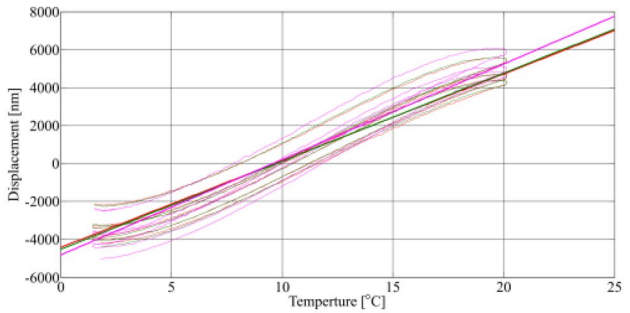

(c) Third experimental result.

Fig. 11 The hysteresis curve of the displacement change with respect to the temperature change of three thermal expansion experiments with the temperature gradient

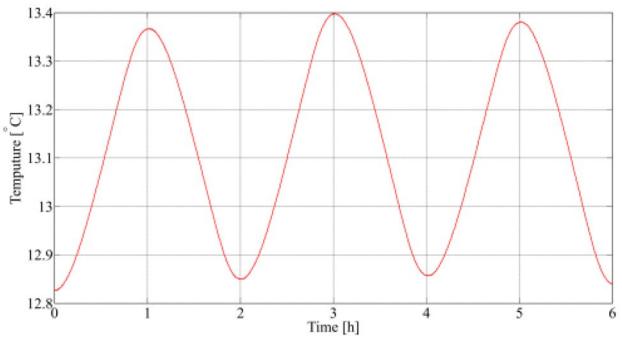

(a) First experimental result.

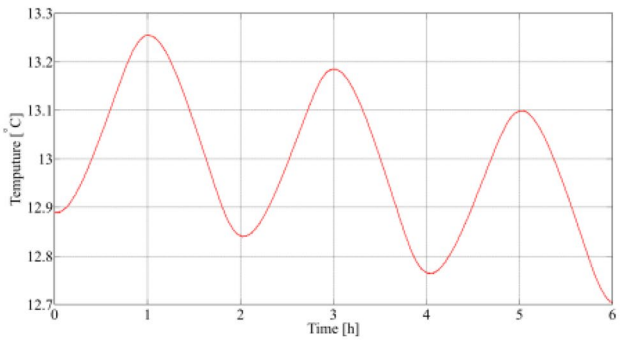

(b) Second experimental result.

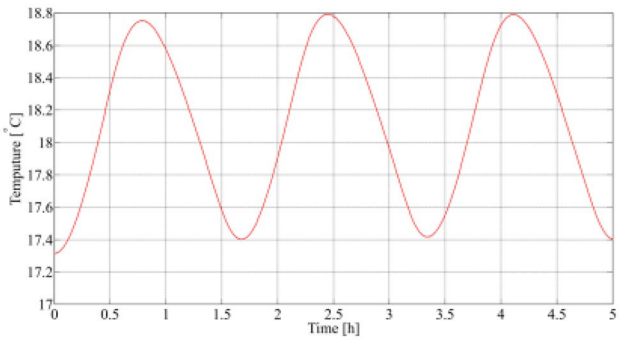

(c) Third experimental result.

Fig. 12 The temperature fluctuations at the lower end of the structure in three thermal expansion experiments with the temperature gradient

maximum error between the three-way measurement results is 6.7%. Under the two kinds of experiments, the measurement errors between the three channels are all within the acceptable range.

In the uniform thermal expansion experiment, the average CTE of the three-way measurement results is 2.32×10^{-7}/K, and the average CTE measured through the thermal expansion experiment with the temperature gradient is 1.24×10^{-6} /K. As shown in Fig. 13, the height between the upper and lower reference mirrors is about 315 mm, and the height ΔH is composed of the transverse thickness of the C/SiC plate. The C/SiC composite used in the design and weaving only ensures that its axial CTE is low, but its transverse CTE is not specially designed, which is why the obtained CTEs of the two kinds of experiments are different.

Suppose the axial and transverse CTE of the C/SiC plate used is x and y, respectively. The total height between the upper and lower mirrors is 315 mm, in which the axial height of the C/SiC plate is 305 mm, and the transverse height is $\Delta H = 10$ mm. In the uniform thermal expansion experiment, the temperature peak value (PV) is 7.5 °C, and the measured distance change is about 1110 nm. In the three experiments with the temperature gradient, the temperature PVs are 3.7 °C, 5.2 °C, 18.5 °C, respectively, and the measured distance change are 1400 nm, 2022 nm, 7474 nm, respectively. Ultimately, we can obtain four binary first-order equations about x and y, as shown in Eq. 8. Using the least square method to perform the linear regression, the solution $x = -8.3 \times 10^{-7}$,

Table 2 The analytical results of the three thermal expansion experiments with the temperature gradient

k[nm/°C]/ CTE[×10^{-6}]	Measurement path 1	Measurement path 2	Measurement path 3	Average
1	371/1.18	388/1.23	406/1.28	388/1.23
2	370/1.17	382/1.21	393/1.24	381/1.20
3	393/1.24	398/1.26	413/1.31	401/1.27
Average	378/1.20	389/1.23	404/1.28	390/1.24

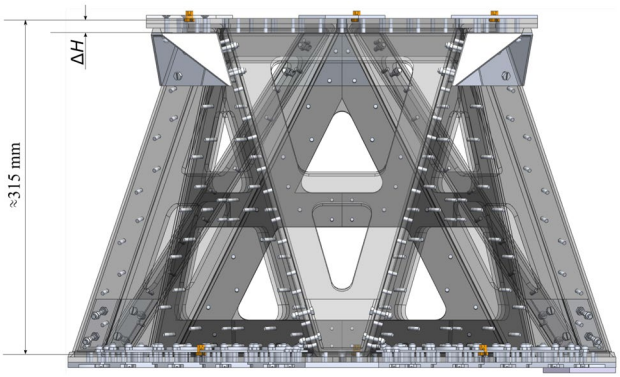

Fig. 13 The CAD model of the C/SiC supporting frame, and ΔH is the transverse thickness of the C/SiC plate

$y = 3.3 \times 10^{-5}$ can be obtained. Thus, we can obtain that the transverse CTE of the C/SiC plate used is about 3.3×10^{-5} /K, and the axial CTE is about -8.3×10^{-7}/K.

$$\begin{aligned} 305 \times 7.5 \times 2 \times x + 10 \times 7.5 \times 2 \times y &= 1.11 \times 10^{-3} \\ 305 \times 3.7 \times x + 10 \times 3.7 \times 2 \times y &= 1.4 \times 10^{-3} \\ 305 \times 5.2 \times x + 10 \times 5.2 \times 2 \times y &= 2.0 \times 10^{-3} \\ 305 \times 18.5 \times x + 18.5 \times 2 \times y &= 7.5 \times 10^{-3} \end{aligned} \tag{8}$$

Conclusion

The requirement accuracy of 1 pm/$\sqrt{\text{Hz}}$ puts forward pretty demanding requirements for the dimensional stability of the telescope in the Taiji program and LISA. The current researches focus on SiC or CFRP, and the relevant research on C/SiC has not been publicly reported. In this paper, the CTE of the telescope supporting frame made of C/SiC composite is measured experimentally. A set of high-precision thermal deformation interferometry system which can measure multiple channels at the same time is designed and built. Using the system, the uniform thermal expansion experiments and the thermal expansion experiments with the temperature gradient are carried out on the C/SiC telescope supporting frame. The CTEs of the overall structure obtained from the two kinds of experiments are 2.32×10^{-7}/K and 1.24×10^{-6}/K, respectively. After analyzing that the difference between the two experimental results is due to the difference between the axial and transverse CTE of the C/SiC plate used, we use the four experimental results to establish the equations for the CTE in two orthogonal directions and use the least square method to obtain the result that the axial and the transverse CTE is approximately -8.3×10^{-7}/K and 3.3×10^{-5}/K, respectively. The picometer-level multi-channel thermal deformation interferometry system designed in this paper can be used for the subsequent thermal performance measurement of the telescope prototype.

As the designed interference measurement structure is large, the interference optical path is long and not placed in the vacuum chamber, the measurement accuracy is not ideal. And due to the limited ports of the phasemeter, it is difficult to measure the Differential Wave-front Sensing (DWS) signal and the OPD signal at the same time, so the attitude change of the supporting frame structure under the thermal deformation cannot be measured at the same time. In order to build the telescope stability detection system of the picometer magnitude, it is necessary to further improve the measurement accuracy of the interference system. For example, the use of all-glass interference optical platform, put in the vacuum chamber for measurement and so on.

Acknowledgements This work was supported by the National Key R&D Program of China (Grant No. 2020YFC2200104) and the Strategic Priority Research Program of the Chinese Academy of Sciences (Grant No. XDA1502110102).

Data Availability The data that support the findings of this study are available from the corresponding author upon reasonable request.

Declarations

Conflict of Interest The authors declare no conflicts of interest.

References

Bender, P., Danzmann, K.: LISA for the detection and observation of gravitational waves. Max-Planck-Institut fur Quantenoptik, Garching Technical Report No. MPQ233 (1998)

Hu, W. R., Wu, Y. L.: Taiji program in space for gravitational wave physics and nature of gravity. Natl. Sci. Rev. (2017)

Livas, J., Sankar, S.: Optical telescope design study results. In Journal of Physics: Conference Series (Vol. 610, No. 1, p. 012029). IOP Publishing (2015)

Livas, J. C., Arsenovic, P., Crow, J. A., Hill, P. C., Howard, J. M., Seals III, L. T., Shiri, S.: Telescopes for space-based gravitational wave missions. Opt. Eng. **52**(9), 091811 (2013)

Livas, J. C., Sankar, S. R.: Optical telescope system-level design considerations for a space-based gravitational wave mission. In Space Telescopes and Instrumentation 2016: Optical, Infrared, and Millimeter Wave (Vol. 9904, p. 99041K). International Society for Optics and Photonics (2016)

Luo, Z., Guo, Z., Jin, G., Wu, Y., Hu, W.: A brief analysis to Taiji: Science and technology. Results in Physics **16**, 102918 (2020)

Luo, Z., Wang, Y., Wu, Y., Hu, W., Jin, G.: The Taiji program: A concise overview. Progress of Theoretical and Experimental Physics **2021**(5), 05A108 (2021)

Machado, J. C., Heinrich, T., Schuldt, T., Gohlke, M., Lucarelli, S., Weise, D., Braxmaier, C.: Picometer resolution interferometric characterization of the dimensional stability of zero CTE CFRP. In Advanced Optical and Mechanical Technologies in Telescopes and Instrumentation (Vol. 7018, p. 70183D). International Society for Optics and Photonics (2008)

Sanjuan, J., Korytov, D., Mueller, G., Spannagel, R., Braxmaier, C., Preston, A., Livas, J.: Note: Silicon carbide telescope dimensional stability for space-based gravitational wave detectors. Rev. Sci. Instrum. **83**(11), 116107 (2012)

Sanjuan, J., Preston, A., Korytov, D., Spector, A., Freise, A., Dixon, G., Mueller, G.: Carbon fiber reinforced polymer dimensional stability investigations for use on the laser interferometer space antenna mission telescope. Rev. Sci. Instrum. **82**(12), 124501 (2011)

Sankar, S., Livas, J.: Testing and characterization of a prototype telescope for the evolved Laser Interferometer Space Antenna (eLISA). In Space Telescopes and Instrumentation 2016: Optical, Infrared, and Millimeter Wave (Vol. 9904, p. 99045A). International Society for Optics and Photonics (2016)

Sankar, S. R., Livas, J. C.: Optical telescope design for a space-based gravitational-wave mission. In Space Telescopes and Instrumentation 2014: Optical, Infrared, and Millimeter Wave (Vol. 9143, pp. 283-289). SPIE (2014)

Sasso, C. P., Mana, G., Mottini, S.: Coupling of wavefront errors and jitter in the LISA interferometer: far-field propagation. Classical Quantum Gravity **35**(18), 185013 (2018)